Phys Chem Minerals (2006) 33: 363–376
DOI 10.1007/s00269-006-0065-2

ORIGINAL PAPER

Anastasia Chopelas

Modeling the thermodynamic parameters of six endmember garnets at ambient and high pressures from vibrational data

Received: 3 March 2005 / Accepted: 9 January 2006 / Published online: 1 August 2006

Abstract Raman and infrared spectroscopic data at ambient and high pressures were used to compute the lattice contribution to the heat capacities and entropies of six endmember garnets: pyrope, almandine, spessartine, grossular, andradite and uvarovite. Electronic, configurational and magnetic contributions are obtained from comparing available calorimetric data to the computed lattice contributions. For garnets with entropy in excess of the computed lattice contribution, the overwhelming majority is found in the subambient temperature regime. At room temperature, the non-lattice entropy is approximately 11.5 J/mol-K for pyrope, 49 J/mol-K for almandine, and 19 J/mol-K for andradite. The non-lattice entropy for pyrope and some for almandine cannot be accounted for by magnetic or electronic contributions and is likely to be configurational in nature. Estimates of low temperature non-lattice entropies for both spessartine and uvarovite are made in absence of calorimetric measurements and are based on low temperature calorimetry of other minerals containing the Mn^{2+} and Cr^{3+} cations as well as on solid solution garnets containing these cations. The estimate for uvarovite non-lattice entropy is approximately 18 J/mol-K, while for spessartine, approximately 45 J/mol-K. Neither of these cations is expected to provide electronic contributions to the entropy. For both iron-bearing garnets, a small electronic or magnetic entropy contribution continues above ambient temperatures. High pressure data on pyrope, grossular and andradite permit calculation of the thermodynamic parameters at high pressures, which are important for computation of processes in the Earth's mantle. Thermal expansion coefficients of these materials were found to be 1.6, 1.5, 1.6×10^{-5} K^{-1} at 298 K, respectively, using a Maxwell relation. These closely match the literature values at ambient conditions.

A. Chopelas
Department of Earth and Space Sciences,
University of Washington,
Box 351310, Seattle, WA 98195-1310, USA
E-mail: chopelas@ess.washington.edu

Introduction

High usage and demand of the current thermodynamic databases clearly underscores the need for modeling of thermodynamic parameters of minerals, particularly their solid solutions. The current petrological internally consistent databases are powerful and do this job very well at ambient and near ambient pressures (Berman 1988; Ghiorso and Sack 1995; Holland and Powell 1998). However, difficulties exist for extrapolations beyond modest (1–2 GPa) pressures. Some work has been done towards these ends (Fabrichnaya 1995; Fei et al. 1990; Ghiorso et al. 2002; Grevel et al. 2001; Kuskov et al. 1983; Saxena et al. 1993), still much work remains. In particular, the internal consistency between the equations of state and the pressure dependence of the entropy, heat capacity and internal energy has not been explicitly addressed.

Garnet solid solutions are a particular challenge even at ambient pressures because of their well-known non-ideal mixing properties (Berman 1990; Ganguly et al. 1996). The thermodynamic properties of garnet solid solutions are of particular interest in many fields of Earth science. Equilibria between garnets and other minerals are the basis for a large number of geothermometers and geobarometers (Ganguly and Saxena 1987). Garnets are important Transition Zone phases for determining composition as well as temperatures. Deviations from ideal mixing properties are the largest for those binary systems in which the mass or size of the cation being substituted varies considerably. A robust modeling of their thermoelastic properties would provide a basis for understanding the solid solution properties at high pressures and can be incorporated into current petrological modeling schemes.

End-member properties provide the starting point for understanding the complex behavior of solid solutions. Contributions to thermodynamic properties are predominantly from the lattice, with magnetic, electronic, configurational, and mixing effects making significant

but smaller contributions. It is not expected that magnetic, electronic, and even mixing contributions to the entropy, for example, to vary greatly with pressure. Virtually all if not all the change in thermodynamic properties will be due to changes in the lattice contribution.

Vibrational modeling provides us with the lattice contribution to the thermodynamic properties. Simpler estimation methods, such as the Debye approximation, are not satisfactory for complex structures with a large number of atoms in the unit cell. Several studies on a large variety of mineral systems have shown the value of vibrational modeling: e.g., Chopelas (1990a, b, 1991, 1999, 2000); Chopelas et al. (1994); Gillet et al. (1991, 1992); Hofmeister (1987, 1996); Hofmeister and Chopelas (1991a). In most of these studies (except Hofmeister 1987) electronic and magnetic contributions to the thermodynamic properties have not been considered.

Vibrational models for both pyrope and grossular end members have been developed (Hofmeister and Chopelas 1991a) These showed that grossular is very well described by considering only the lattice contribution for its properties, while the non-lattice heat capacity of pyrope at low temperatures requires additional contributions, such as configurational or dynamical disorder. The vibrational properties of the four other endmember garnets have now been well investigated (Chopelas 2005; Hofmeister and Chopelas 1991b; Kolesov and Geiger 1998; Moore and White 1971). The essential low-temperature calorimetry has been done on the iron-bearing garnets of almandine and andradite (Anovitz et al. 1993; Robie et al. 1987), while only the high-temperature heat capacity of spessartine has been measured (Geiger and Armbruster 1997). The only calorimetric information on uvarovite exists on dilute solutions containing pyrope and almandine as major components (Kolesnik et al. 1994). High-pressure Raman spectroscopic data exist for pyrope, grossular, and andradite (Gillet et al. 1992; H.J. Reichmann and A. Chopelas, unpublished data).

In this paper, we use the previously developed vibrational models (Hofmeister and Chopelas 1991a) to compute the lattice contribution to the thermodynamic properties of almandine, andradite, spessartine, and uvarovite. Vibrational modeling with the existing spectroscopic and calorimetric data for garnets will provide: (1) a solid basis for determining the electronic, configurational, and magnetic contributions to the heat capacity and entropy for the iron-bearing garnets, (2) good estimates on the magnetic, configurational, and electronic contributions of the remaining two endmember garnets, (3) the ability to calculate the high-pressure properties of three garnets, (4) estimates of thermal expansivity on these same three garnets using a Maxwell relation (Chopelas 1996, 2000), (5) further internal consistency checks between volumes at pressure and temperature using the pressure dependence of the heat capacity and internal energy, and (6) a solid basis for computing the thermodynamic properties of solid solution mixtures once their spectra are known. Future work in this area will use our new results on Raman spectra of binary garnet solutions (Savage and Chopelas 2002, 2003) as well as previously reported Raman and infrared studies (Boffa Ballaran et al. 1999; Geiger 1998; Hofmeister et al. 1996; McAloon and Hofmeister 1995; Rodehorst et al. 2004).

Methodology

The vibrational models used to calculate the lattice contribution to the thermodynamic properties were developed by careful enumeration of the modes using symmetry analysis, factor group analysis, and mode assignments based on cation or isotopic substitution, high pressure, as well as variable temperature measurements of the vibrational modes. The previous models for pyrope and grossular are modified by adjusting the ranges of the model using the spectroscopic data (Hofmeister and Chopelas 1991a). The models are shown in Table 1. Table 2 lists the parameters used in the calculations. The required spectroscopic data are taken from (Chopelas 2005; Hofmeister and Chopelas 1991b; A.M. Hofmeister, unpublished data).

Using statistical methods, the constant volume heat capacity C_V is estimated from

$$C_V = 3Nk \int_0^\infty \frac{e^x}{(e^x - 1)^2} x^2 g(\nu) d\nu \quad (1)$$

where N is the number of atoms in the unit cell, k Boltzmann's constant, ν the frequency of vibration, x is $h\nu/kT$, h Planck's constant, and $g(\nu)$ the density of states. C_V is converted to the constant pressure heat capacity C_P using

$$C_P = C_V + TV\alpha^2 K_T \quad (2)$$

which may also be expressed as $C_P = C_V (1 + \alpha\, \gamma_{th}\, T)$ or $C_P = C_v + \alpha\gamma_{th}\ C_v\ T$, where $\gamma_{th} = \alpha\ K_T V/C_V$. The "anharmonic" correction "$\alpha\gamma_{th}T$" is very small until about 700 K. By 1,000 K, it is about 5% of the total value of the heat capacity, most of which is due to the contribution from T.

Values of thermal expansion, bulk modulus, and molar volumes for each of the garnets are summarized in Table 1. At high temperatures, γ_{th} and α vary little with pressure and temperature (Anderson et al. 1991). At high pressures, α varies with volume according to $-\partial \ln \alpha/\partial \ln V = \delta_T$ and γ_{th} is varied with density assuming $\gamma_{th}\rho$ = constant. The soundness of the vibrational models are checked for consistency by: (1) the comparison of calorimetric data to those obtained using Eqs. 1 and 2, as done previously for all materials, (2) and where available, comparison of the spectroscopically derived weighted average Grüneisen parameter

Table 1 Vibrational models for six garnets. Volumes and thermal expansion are from Skinner (1956) and Bass (1986), bulk moduli from Bass (1986), Zhang et al. (1998, 1999), and thermal expansion adapted from Skinner (1956), Tequi et al. (1991), Thieblot et al. (1999) to allow accuracy at high temperatures in the models. Vibrational frequencies are from Chopelas (2005), Hofmeister and Chopelas (1991b)

Number of modes	Lower limit (cm^{-1})	Upper limit (cm^{-1})	γ_i	Mode type
Grossular				
1	0	74	1.4	A
1	0	74	1.4	A
1	0	126	1.7	A
33	159	330	1.4	C
36	178	249	1.05	C
24	245	474	1.55	C
36	349	406	1.2	C
24	416	549	0.9	C
36	505	631	0.85	C
20	847	849	0.8	E
12	865	867	0.75	E
6	903	905	0.8	E
10	974	976	0.7	E
a (A)		11.841		
Ko (GPa)		170		
K′		5.2		
α (10^{-6}/K)		20 + 0.01×T		
γ_{th}	1.14			
$\langle\gamma\rangle$	1.145			
Pyrope				
1	0	73	1.7	A
1	0	73	1.7	A
1	0	130	1.9	A
33	140	342	1.4	C
36	200	272	1.2	C
24	279	478	1.3	C
36	350	400	1.5	C
24	439	562	0.9	C
36	510	667	0.85	C
20	889	891	0.8	E
12	917	919	0.6	E
6	937	939	0.7	E
10	1029	1031	0.8	E
a (A)		11.455		
Ko (GPa)		171		
K′		4.4		
α (10^{-6}/K)		18 + .012×T		
γ_{th}	1.13			
$\langle\gamma\rangle$	1.13			
Andradite				
1	0	67	1.6	A
1	0	67	1.6	A
1	0	118	1.9	A
33	152	311	1.4	C
36	173	247	0.9	C
24	133	359	1.45	C
36	322	418	1.6	C
24	352	516	0.9	C
36	479	593	0.85	C
20	821	823	0.8	E
12	843	845	0.75	E
6	873	875	0.7	E
10	949	951	0.5	E
a (A)		12.054		
Ko (GPa)		162		
K′		4.2		
α (10^{-6}/K)		20 + 0.01×T		
γ_{th}	1.15			
$\langle\gamma\rangle$	1.17			
Almandine				
1	0	68		A
1	0	68		A
1	0	122		A
33	111.5	326		C
36	137.5	212		C
24	236	467.7		C
36	312	396		C
24	421	553		C
36	498	634.5		C
20	861	863		E
12	909	911		E
6	919	921		E
10	999	1001		E
a (A)		11.52		
Ko (GPa)		185		
K′		4.2		
α (10^{-6}/K)		18 + 0.015×T		
Spessartine				
1	0	74		A
1	0	74		A
1	0	126		A
33	112	318		C
36	140.5	220		C
24	246	461.4		C
36	314	383		C
24	410	550		C
36	499	630		C
20	848	850		E
12	897	899		E
6	912	914		E
10	1000	1002		E
a (A)		11.607		
Ko (GPa)		183		
K′		5.1		
α (10^{-6}/K)		21 + 0.01×T		
Uvarovite				
1	0	67		A
1	0	67		A
1	0	119		A
33	142	330		C
36	178	241		C
24	300	440		C
36	338	377		C
24	398	517		C
36	530	618		C
20	833	835		E
12	865	867		E
6	891	893		E
10	953	955		E
a (A)		12.02		
Ko (GPa)		165		
K′		4.7		
α (10^{-6}/K)		21 + 0.01×T		

$\langle\gamma\rangle = \sum C_i\ \gamma_i / \sum C_i$, where C_i is the Einstein heat capacity and γ_i the mode Grüneisen parameter of mode i, to γ_{th} obtained as earlier. This check can only be performed on pyrope, grossular, and andradite since high pressure spectroscopic data is lacking or insufficient for the others.

The following equation is integrated over temperature to obtain the third law entropy:

Table 2 Plug in values for the vibrational models and correction of C_V to C_P

	a (A)	V_L (A^3)	v_p (km/s)	v_s (km/s)	ρ (g/cm^3)	v_1 (cm^{-1})	v_2 (cm^{-1})
Pyrope	11.45	751.4	8.942	5.021	3.602	72.77	129.6
Almandine	11.52	764.3	8.328	4.636	4.3	66.81	120
Spessartine	11.61	781.8	8.58	4.76	4.195	68.08	122.7
Grossular	11.84	830.1	9.101	5.234	3.6	73.38	127.6
Andradite	12.05	875.7	8.492	4.728	3.859	65.12	117
Uvarovite	12.02	868.3	8.602	4.834	3.85	66.77	118.8

$$\Delta S = \int_0^{T_1} \frac{C_P}{T} \mathrm{d}T, \tag{3}$$

where T_1 is the temperature of interest.

It was shown by Chopelas (1996) that thermal expansivity may be well constrained by using information obtained from vibrational spectroscopy at high pressure. The advantage of this method is that the measurements are performed at room temperature and the frequencies versus pressure are very precisely determined. In all cases, several measurements were taken within the stability field of the phase. The variation of frequency with pressure provides a basis for estimating entropy versus pressure, which directly yields thermal expansivity through the Maxwell relation

$$\left(\frac{\partial V}{\partial T}\right)_P = -\left(\frac{\partial S}{\partial P}\right)_T, \tag{4}$$

where S is entropy, V volume, P pressure, and T temperature. To estimate entropy at higher pressures, the frequencies in the vibrational models (Table 1) are shifted in accordance with measurements of $v(P)$, as represented by the mode Grüneisen parameters $\gamma_i = (K_T/v_0)(\partial v/\partial P)_T$ assigned to each frequency range. Fundamentally the resulting value of α depends on v(P). Entropy as a function of pressure is fitted to a second-order polynomial for use in Eq. 4. Thermal expansivity is then

$$\alpha = \frac{1}{V}\left(\frac{\partial V}{\partial T}\right)_P \tag{5}$$

To calculate α from the variation of entropy versus pressure, the molar volume of the phase must be known at the pressure and temperature of interest. Since α is used to calculate C_P, the results from Eq. 5 are substituted back into Eq. 2. The process is continued by successive iteration until convergence occurs.

Further consistency checks between volumes at various pressure and temperature conditions can be made using the pressure dependence of both the heat capacity and internal energy (integration of the C_v with respect to temperature). Through a Maxwell relation, we have

$$\left(\frac{\partial C_P}{\partial P}\right)_T = -T\left(\frac{\partial^2 V}{\partial T^2}\right)_P \tag{6}$$

The thermal pressure, $P_{\mathrm{TH}} = (\partial P/\partial T)_V$, is related directly to the vibrational internal energy through

$$P_{\mathrm{TH}} = \frac{1}{V} \times \sum_i \gamma_i E_i, \tag{7}$$

which is also known in its familiar Mie Grüneisen form of $P_{\mathrm{TH}} = \gamma\ E_{\mathrm{vib}}/V$. In both these cases, the volume of a material at pressure and temperature is directly related to the vibrational spectrum. These relations provide additional internal consistency checks of the available thermoelastic data on any material.

Construction of the density of states

The cubic garnet structure Ia3d, formula $X_3Y_2Si_3O_{12}$ consists of a three-dimensional network of alternate corner linked SiO_4 tetrahedra and YO_6 octahedra. In this study, X = divalent cations of Mg, Ca, Mn, or Fe, while Y = trivalent cations of Al, Fe, and Cr. Analysis of variations in the spectrum by substitution of cations and isotopes or by varying pressure and temperature helps establish extent of each motion in a structure which contributes to a particular vibrational mode. The purpose for determining contribution is to construct a reasonable density of states for thermodynamic calculations by ascertaining where the silent modes would appear. This approach has been very successful in the past for constructing reasonable models that accurately predict thermodynamic functions, such as heat capacity, entropy, thermal expansivity, and relative compressibility, particularly for pyrope and grossular (Hofmeister and Chopelas 1991a).

Symmetry analysis predicts 25 Raman active modes: 3 A_g, 8 E_g, and 14 T_{2g}, which have been observed for the six end-member garnets in this study. Detailed factor group analysis shows there are 14 modes that should be in the high-energy part of the spectrum receiving contributions primarily from the silica tetrahedra, divided between stretching and bending motions. In the set of low-energy modes, symmetry analysis shows that there are further 8 modes that are due to translations and rotations of the SiO_4 structural unit. There are only 3 modes attributed to the divalent cation or X translation. Translations of the trivalent or Y cation are not Raman active. The observations by cation and isotope substitution in garnets agree loosely with this analysis (Hofmeister and Chopelas 1991b; Kolesov and Geiger 1998, 2000) except that the external modes show behavior upon substitution that demonstrate they are of mixed character. The approximate character of the

mode assignments is rather for accounting and establishing frequency ranges for the various types of modes so that the silent modes can be estimated appropriately for use in vibrational modeling. Macroscopic thermodynamic properties can then be derived accurately from the microscopic vibrational properties.

Our previous work shows that infrared spectra have very similar mode frequencies to Raman modes for the same molecular motion as well as contain translations of the trivalent (Y) cation in its octahedral site so it strengthens our ability to construct a robust density of states for thermodynamic calculations (Hofmeister and Chopelas 1991b).

Non-lattice contributions to thermodynamic properties

Neither pyrope nor grossular have transition metals that can contribute to the heat capacity or entropy via antiferromagnetic ordering or electronic configuration. Pyrope does have an added contribution at low temperatures believed to be due to the size mismatch between the small Mg^{2+} cation and the eightfold coordinated site (Haselton and Westrum 1980; Kolesov and Geiger 2000). The remaining four garnets contain transition metals that can contribute, mainly as magnetic transitions of antiferromagnetic ordering of the spins in iron, manganese, or chromium.

The maximum contributions of magnetic entropy per mole can be easily ascertained by $R \ln(2S + 1)$, where S represents the number of unpaired spins in the transition metal cation. For almandine, the maximum is 40.1 J/mol-K, for andradite 29.8 J/mol-K, for spessartine 44.7 J/mol-K, and for uvarovite 23.1 J/mol-K. If short range magnetic order persists above the transition temperature (Nèel temperature T_N), the maximum entropy contribution may not be fully realized. In crystals where the transition metals are substantially diluted, like the garnets, the Néel temperatures tend to be very low (substantially below 100 K). The transition shows up as a spike in the heat capacity curve. In almandine, this occurs at 8.5 K (Anovitz et al. 1993) and in andradite, at 11.7 K (Robie et al. 1987).

Further contributions to entropy could be found in almandine garnets which contain Fe^{2+} (d^6 electron configuration) and have the possibility of an additional electronic contribution to the entropy due to the configuration of the electrons in their bonding orbitals, $3R \ln 2 = 17.3$ J/mol-K for almandine (Ulbricht and Waldbaum 1976). The full contribution to entropy may not be realized if the bonds around the divalent iron are not the same length, hence the site is not a regular dodecahedron. The contribution will generally increase with rising temperature as the dodecahedral site becomes more regular and the energy splitting of the bonding orbitals due to site distortions decreases.

Calculation of the lattice contribution to the heat capacities and entropies of the six end-member garnets allows an accurate assessment of the electronic and magnetic contributions for these materials by comparison to the calorimetric results.

Results and discussion

The vibrational models for garnets used in the present calculations are shown in Table 1. The other required parameters, thermal expansivity, bulk modulus, its pressure derivative, and Grüneisen parameter, are also listed.

Grossular: $Ca_3Al_2Si_3O_{12}$

Grossular's contribution to the thermodynamic parameters should be only from the lattice. There are several calorimetric measurements on grossular and they all agree with one another (Geiger and Armbruster 1997; Haselton and Westrum 1980; Krupka et al. 1979; Thieblot et al. 1999). Heat capacities and entropies of vibrational modeling are an exact match to these data. (Hofmeister and Chopelas 1991a). The model calculations are extended to show that they agree with newer Cp data up to 1400 K (Thieblot et al. 1999). The various calorimetric studies are shown in Fig. 1a, and the differences between the calorimetric and lattice heat capacities are shown in Fig. 1b. It is not surprising that at temperatures below 50 K, the lattice heat capacity differs from the calorimetric heat capacity. These differences can be attributed to differences between the actual vibrational spectrum and the vibrational model around 50 cm^{-1}. There is no bias in the differences as it can be seen in the entropy calculation. It is clear that these differences are not biased towards non-lattice heat capacity as it can be seen in the entropy calculation. The entropy calculated from vibrational modeling is nearly identical to that from calorimetric heat capacity data from about 50 K to the highest temperature of the calorimetric data (Fig. 1c), which is not true for any of the other garnets (see subsequently). Any difference of the computed from the calorimetric data are well within the scatter of the data and their uncertainties.

Clearly there are no other factors contributing to the thermodynamic properties of grossular beyond those from the lattice. The remaining end-member garnets in this study have other contributions to their thermodynamic properties as follows.

Pyrope: $Mg_3Al_2Si_3O_{12}$

Although pyrope does not have any transition metals which would contribute either electronically or magnetically to the entropy and heat capacity, an anomalously high C_P has been measured calorimetrically below 200 K. As noted by Haselton and Westrum (1980), the C_P of pyrope unexpectedly exceeded that of grossular despite anticipating that the lighter magnesium cation (compared to calcium) would produce the opposite

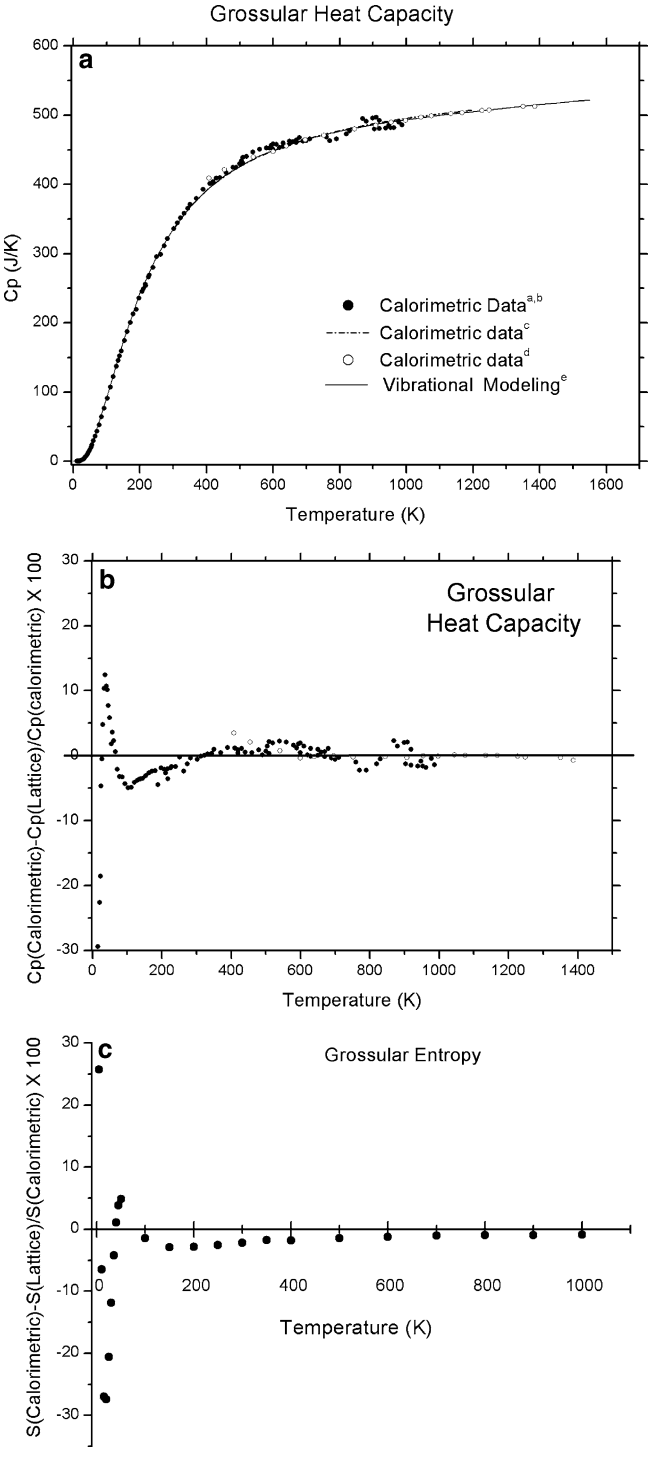

Fig. 1 **a** The constant pressure heat capacity versus temperature for grossular. The *solid line* is from vibrational modeling (*e*: this study). Calorimetric data: (*a*) Haselton and Westrum Jr. (1980), (*b*) Krupka et al. (1979), (*c*) Thieblot et al. (1999), (*d*) Geiger and Armbruster (1997). The points are calorimetric data listed in the sources. The *dotted line* represents a best fit to their data. The spread of the data is similar to that listed earlier. **b** The percent difference between the calorimetric heat capacity of grossular from Fig. 1a and the lattice heat capacity from vibrational modeling (this work) versus temperature. Above 200 K, the differences are no more than 2% and vary above as much as below the line. Below 200 K, the differences are exaggerated by the very low values of heat capacity and the inability of the simple models to mimic actual vibrational spectra below 100 cm^{-1}. The variation is below as well as above the lattice calculation. **c** The percent difference between calorimetric entropy of grossular to the lattice entropy versus temperature. Above 50 K, this value is always less than 1.5%. Above 400 K, the agreement improves. There are no other obvious contributions to the thermodynamic properties of grossular

effect. This anomalously high heat capacity was also seen in earlier measurements on solid solutions with a high pyrope content (Kolesnik et al. 1994). The mismatch between the small Mg cation and the large 8-coordinated dodecahedral site is the most cited cause for the non-lattice entropy. Recently Raman measurements at cryogenic temperatures show that the low-energy mode at about 140 cm^{-1} persists down to the lowest temperature of their study and shifted substantially with isotopic substitution of magnesium (Kolesov and Geiger 2000). The authors proposed a dynamic disorder rather than a configurational disorder of the magnesium in the garnet lattice. The vibrational model for pyrope has been adjusted from the original work (Hofmeister and Chopelas 1991a) to accommodate the observed vibrational mode (Table 1). It still did not reproduce the anomalously high heat capacity (shown in Fig. 2a, b). Examination of the difference between the calorimetric measurements and the vibrational modeling results (Fig. 2b), it is clear that the primary differences is below 200 K, peaking at about 90 K. The difference is clearly seen by comparison of the calorimetric entropy to the one obtained by vibrational modeling (Fig. 2c). An entropy difference of 11.5 J/mol-K is attained by 200 K, as clearly shown in the figure, and then maintained to the highest temperatures of 1,800 K. So, here, the only other contribution to the thermodynamic properties is a small but constant value saturating below 200 K. Closer examination of the thermodynamic properties of solid solutions should help determine the extent that the lattice dilation caused by partial substitution of larger cations into pyrope will affect the magnitude of the entropy difference. There are no magnetic or electronic contributions to the thermodynamic properties of pyrope.

Andradite: $Ca_3Fe_2Si_3O_{12}$

Andradite differs from grossular by the substitution of the d^5 transition metal Fe^{3+} into its octahedral site, which results in extra contributions to the entropy and heat capacity beyond those from the lattice. The five half-full *d* orbitals in ferric iron do not add any electronic configurational entropy to andradite. Andradite undergoes antiferroelectric ordering with a Néel temperature of 11.5 K (Robie et al. 1987) which contributes to the heat capacity as a lambda transition (spike) in the heat capacity curve at 11.7 K. The maximum amount of magnetic entropy that trivalent iron can contribute to

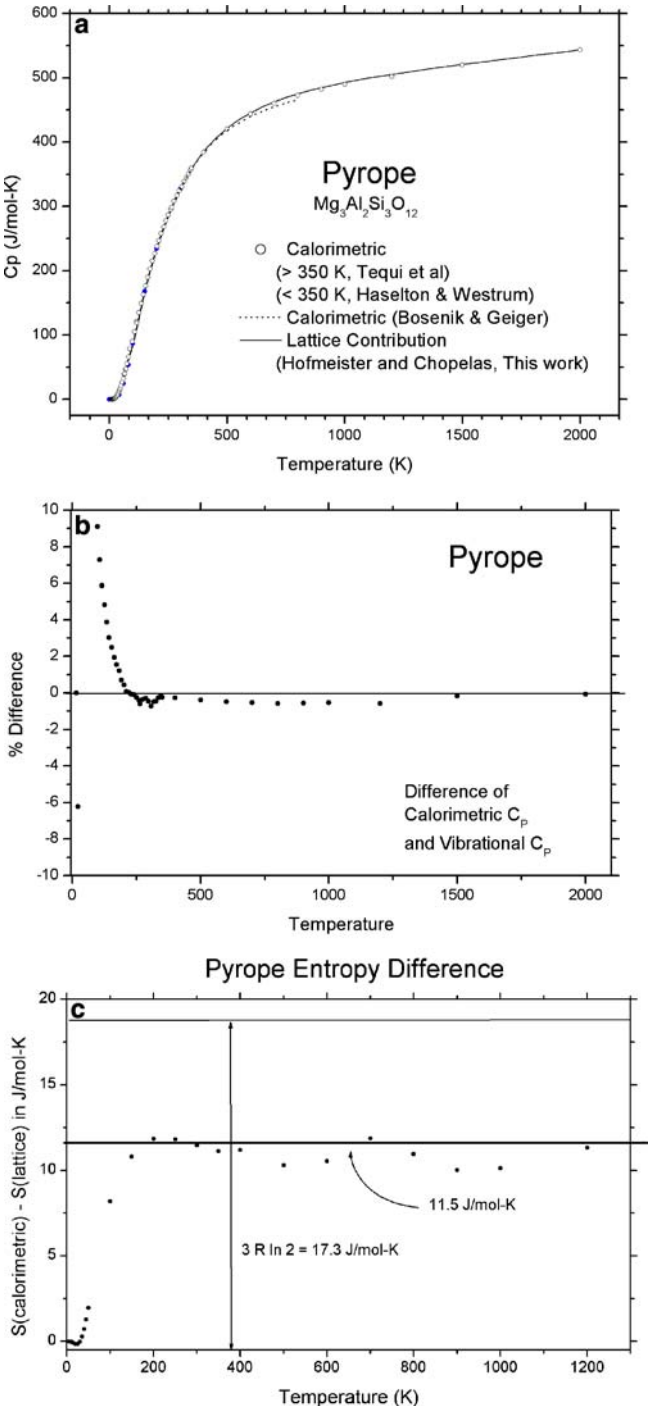

Fig. 2 **a** The constant pressure heat capacity versus temperature for pyrope. The *solid line* is from vibrational modeling (this study). Calorimetric data: Haselton and Westrum Jr. (1980), Tequi et al. (1991), Bosenick et al. (1996). The *points* represent individual data points listed in the sources. **b** The percent difference between the calorimetric heat capacity of pyrope from (**a**) and the lattice heat capacity from vibrational modeling (this work) versus temperature. Above 250 K, the differences are less than 1%. Below 250 K, there is clearly a much higher measured heat capacity than accounted for by the lattice. **c** The percent difference between calorimetric entropy of pyrope to the lattice entropy versus temperature. There is a rapid rise in entropy above the lattice value to 11.5 J/mol-K at 200 K, which then remains constant to the highest temperatures. This added entropy is not accounted for by the peak found at 140 cm^{-1} in the Raman spectrum of pyrope. A configurational disorder with two positions could contribute a maximum entropy of $3R$ ln 2 = 17.3 J/mol-K, indicated in the figure

the heat capacity is $2R$ ln(2S + 1), where the spin quantum number $S = 5/2$, or 29.8 J/mol-K. The maximum contribution occurs only when all antiferromagnetic ordering is randomized. Often residual short-range order remains, thus the maximum contribution to the entropy is not attained. A comparison of C_P from vibrational modeling and that measured by calorimetry is shown in Fig. 3a and their difference in Fig. 3b. In this plot, it is obvious that the difference between the measured and calculated heat capacities (Fig. 3b) spikes at 11.7 K and returns almost immediately to zero. Above room temperature, there is a gradual rise in the difference by up to 10 J/mol-K. The rise is well outside the experimental uncertainties or the uncertainties in the thermoelastic parameters used to correct C_v to C_p using Eq. 2. Examination of the difference between the lattice contribution to entropy and the calorimetric entropy shows a sharp rise to 15 J/mol-K at 20 K, a leveling off to 19 J/mol-K by 100 K, then a slow and steady rise starting above 300 K to 24 J/mol-K at 1,000 K. This is still less than the maximum possible magnetic entropy contribution. Possible reasons could be: (1) the lack of calorimetric data below 9.7°, which may lead to an underestimate of the entropy, (2) significant amount of short range order is retained by the spins well above T_N.

The gradual rise in the entropy difference (Fig. 3c) in andradite above 300 K is not seen in spessartine (the divalent manganese is also a d^5 transition metal) or other Mn^{2+} minerals such as tephroite (A. Chopelas, unpublished work). It is unlikely to be an intrinsic anharmonic contribution (that due to temperature rather than volume) since grossular, pyrope or spessartine show no such contributions to their high temperature thermodynamic properties. It could be due to the gradual disordering of the antiferromagnetic ordering or some other disorder within the lattice. This needs to be explored further. Nonetheless, clear difference between the calculated lattice and measured calorimetric thermodynamic properties allows a reasonable approach to estimating the contribution of ferric iron to the thermodynamic properties of garnets. This concept is pursued further in our recent solid solution Raman studies (A. Chopelas, unpublished manuscript) but reported in abstract form (Savage and Chopelas 2002; Savage and Chopelas 2003).

Almandine: $Fe_2Al_2Si_3O_{12}$

The difference between pyrope and almandine is the substitution of the d^6 ferrous iron for magnesium. The unit cell volumes between almandine and pyrope are similar (Table 1), but the iron cation is slightly larger

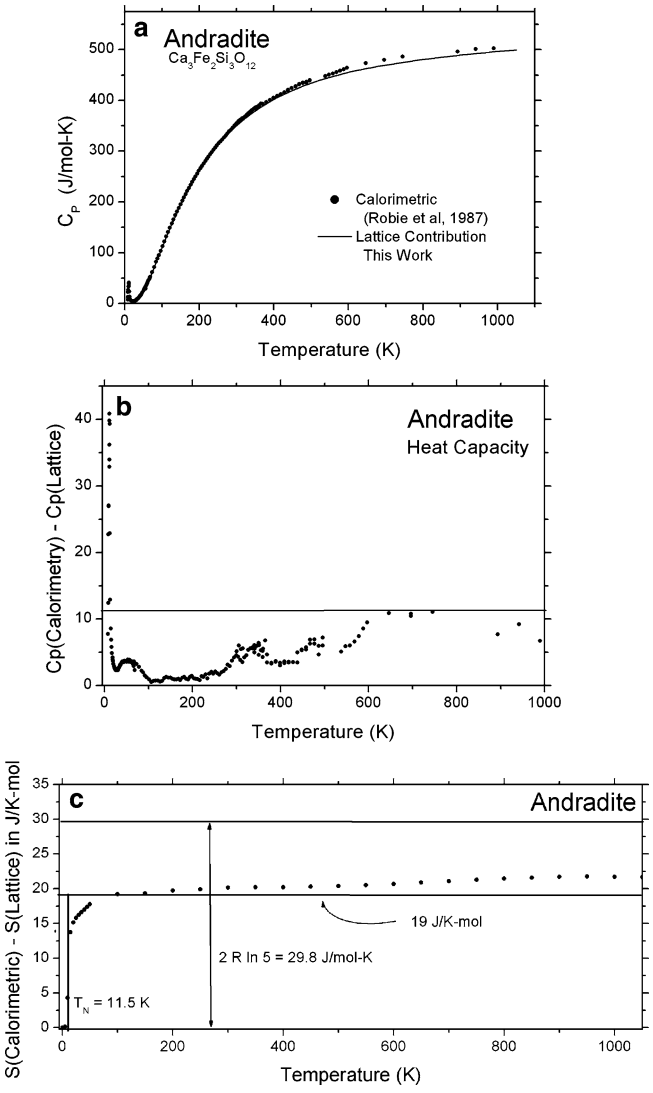

Fig. 3 **a** The constant pressure heat capacity versus temperature for andradite. The *solid line* is from vibrational modeling (this study). Calorimetric data: Robie et al. (1987). The points are calorimetric data listed in the reference. **b** The difference between the calorimetric heat capacity of andradite from (**a**) and the lattice heat capacity from vibrational modeling (this work) versus temperature. The antiferromagnetic transition of the iron is shown as a spike at very low temperatures. Directly afterwards, the lattice and calorimetric Cp are nearly identical. Above room temperature, the difference climbs gradually to a maximum difference of 10 J/mol-K. **c** The difference between calorimetric entropy of andradite to the lattice entropy versus temperature. There is a rapid rise in entropy above the lattice value at 11.5 K, the Néel temperature. It reaches a value of 19 J/mol-K at just below 100 K. Above room temperature, this value rises to 23 J/mol-K at 1,000 K. The maximum possible magnetic entropy of 29.8 J/mol-K is indicated

and may be a better fit into the 8-coordinated dodecahedral site. The following discussion may cast some doubt on this.

Like ferric iron, ferrous iron displays anti-ferromagnetic ordering with a Néel temperature of 7.5 K, which is reflected in the heat capacity measurements as a lambda transition at about 8.5 K. The maximum magnetic contribution to the entropy that the ferrous iron can contribute is $3R$ ln 5 or 40.1 J/mol-K. In addition to the magnetic contribution, the distribution of electrons in divalent iron can contribute an additional $3R$ ln 2 or 17.3 J/mol-K in electronic entropy, for a maximum total of 57.3 J/mol-K. The latter electronic contribution is not usually seen to any large degree because the cation sites in these and other low-symmetry minerals have cation–oxygen bonds that are of different length, leading to a reduction of symmetry and a loss of this contribution to the thermodynamic properties. At higher temperatures, the bonds may become more equal and the site more symmetric, thus allowing some electronic contribution to the entropy: see discussion in Wood (1981).

Comparison of the lattice contributions to the heat capacity and the calorimetric measurements (Anovitz et al. 1993) show a substantial difference in the 0–40 K temperature range (Fig. 4a). Above room temperature, a small but persistent non-lattice C_P is also shown in the measurements. A plot of the differences reveals details otherwise not easily seen (Fig. 4b). Unlike the analogous plot for andradite, the non-lattice heat capacity does not drop immediately to zero but rather there is a broad shoulder that remains until nearly room temperature. This shoulder is very similar to that exhibited by pyrope, which has been attributed to the size mismatch between the "too small" magnesium cation and large dodecahedral site. In pyrope, similar to almandine, the maximum is at approximately 60 K and decreases towards zero at about 150 K. However, the shoulder in the almandine plot is miniscule in comparison to that of pyrope but may still be a small source of entropy.

A plot of the difference between the lattice entropy and calorimetric entropy shows a sharp climb of entropy at low temperatures to about 49 J/mol-K where it levels off above 200 K. The entropy difference then climbs slowly to a maximum value of 53 J/mol-K at 1,000 K. The initial entropy difference climb to 49 J/mol-K is unusually high and was noted in the calorimetric study (Anovitz et al. 1993). However, it was speculated that this may be due to disorder in the electrons which contributes $3R$ ln $2 = 17.3$ J/mol-K to the entropy (as a Schottky anomaly, which is driven by crystal defects). The shape of the non-lattice heat capacity, here, vaguely resembles that found for materials with Schottky defects (Drulis et al. 2002).

Another possible contribution could be due to the electron configurational entropy (Ulbricht and Waldbaum 1976). This is unlikely because it requires the A site in the almandine structure to be regular with all metal oxygen bonds to be of same length at very low temperatures. Then, it should manifest itself as a non-zero entropy at near absolute zero temperature and not to be apparent in the calorimetric heat capacity measurements which start at a higher temperature. If it were to manifest itself at higher temperatures, it would occur gradually adding a small contribution over a larger temperature range (Wood 1981).

A third explanation for the added entropy and heat capacity could be the same as for pyrope, that the Fe^{2+}

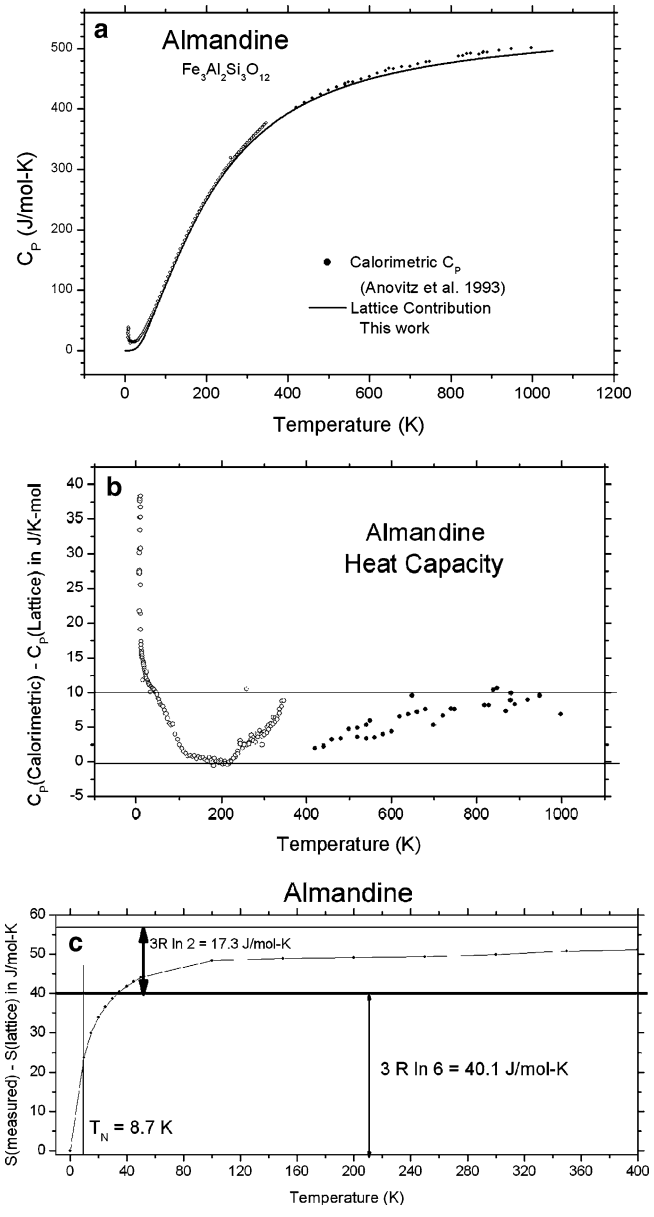

Fig. 4 **a** The constant pressure heat capacity versus temperature for almandine. The *solid line* is from vibrational modeling (this study). Calorimetric data: Anovitz et al. (1993). The points are calorimetric data listed in the reference. **b** The difference between the calorimetric heat capacity of almandine from (**a**) and the lattice heat capacity from vibrational modeling (this work) plotted versus temperature. The antiferromagnetic transition of the iron is shown as a spike at very low temperatures. Directly afterwards, a difference remains to about 100 K and then drops to zero. Above room temperature, the difference climbs gradually again to a maximum of 10 J/mol-K. **c** The difference between calorimetric entropy of almandine to the lattice entropy plotted versus temperature. There is a rapid rise in entropy above the lattice value at 8.5 K, the Néel temperature. It reaches a value of 49 J/mol-K at just below 100 K, which exceeds the maximum entropy of 40.1 J/mol-K anticipated from the antiferromagnetic ordering occurring at 8.5 K. Above room temperature, this value rises further to 53 J/mol-K at 1,000 K. A second limit of $3R$ ln 2 is shown, which would be the added entropy of a Schottky-type anomaly or the electronic entropy of the d^6 Fe^{2+}

cation is smaller than the dodecahedral site and has a contribution to entropy either due to a configurational component or due to a dynamic disorder. The amount of the non-lattice entropy (about 10 J/mol-K) is of the same magnitude as that for pyrope. A good test would be an examination of the low temperature heat capacity of spessartine since it has a nearly equal small cation as Fe^{2+} residing in the dodecahedral site. It is interesting to note that neither almandine nor spessartine shows the Raman mode at 140 cm^{-1} (or its equivalent at about 90–95 cm^{-1} taking into consideration the increased mass of the iron or manganese).

Spessartine: $Mn_3Al_2Si_3O_{12}$

The calorimetric data on spessartine is limited to a set of differential scanning measurements from 350 to 950 K (Geiger and Armbruster 1997). The computed lattice C_P agrees perfectly with this data, falling well within their stated uncertainties; thus, there are no obvious non-lattice contributions to the heat capacity at these temperatures (see Fig. 5a, b). Similarly, in other manganese containing minerals, such as tephroite and rhodochrosite (Robie et al. 1982, 1984), lattice contributions to the heat capacity match the available high temperature heat capacity data (A. Chopelas, unpublished work).

At much lower temperatures, it is expected that Mn^{2+} in spessartine to have a magnetic contribution to the entropy from antiferromagnetic ordering. Antiferromagnetic ordering occurs in tephroite (Mn_2SiO_4), rhodochrosite ($MnCO_3$), and braunite (Mn_7SiO_{12}). These appear as lambda forms in the heat capacity curves at 47.4 K, 34.3 K, and 94 K, respectively (Robie et al. 1982, 1984, 1995), which are very close to their iron-bearing equivalents (ibid.). Since the divalent manganese cation has 5 unpaired d electrons in the high spin state, the maximum size of the entropy contribution is expected to be $3R$ ln 6 or 44.7 J/mol-K. In other manganese containing materials, the maximum non-lattice entropy is reached by about double the Néel temperature. If the iron-bearing garnets are any indication, the transition or Néel temperature should be between 5 and 20 K. It could be higher, see the discussion on uvarovite in the following section. There is no electronic contribution expected from the divalent manganese because in the high spin state, the 5 d electrons have a unique configuration.

There might be one further contribution to the entropy based on the observations for pyrope and almandine. The ionic radius of 8-coordinated Mn^{2+} is very close to that for Fe^{2+} and Mg^{2+} (110 to 106 pm and 103 pm, respectively). There could be a contribution in the 50 to 150 K range due to the "size mismatch" factor mentioned for pyrope and possibly in almandine (if no other cause can be found). Before low temperature calorimetry experiments are performed on spessartine,

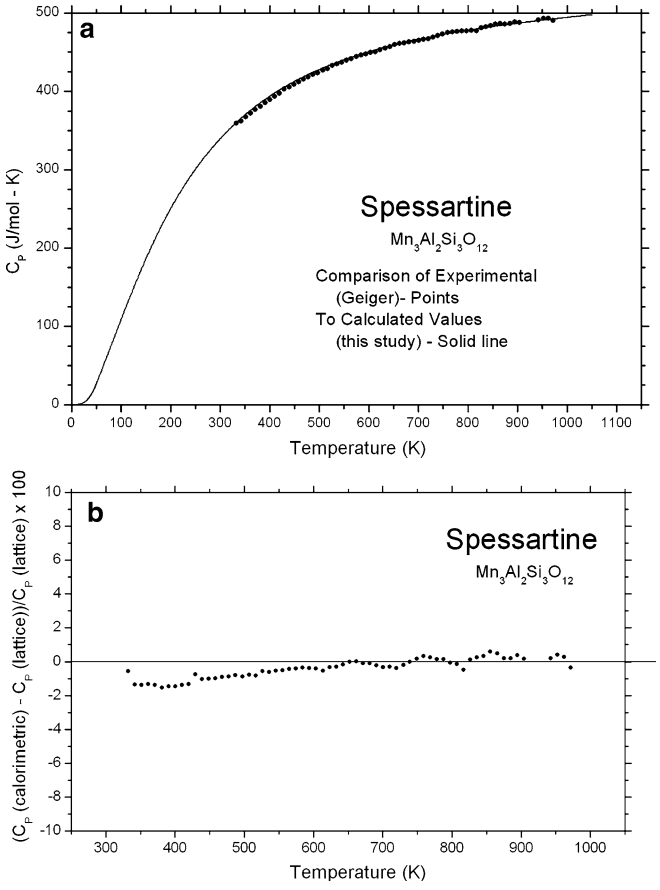

Fig. 5 **a** The constant pressure heat capacity for spessartine plotted against temperature. The *solid line* is from vibrational modeling (this study). Calorimetric data: Geiger and Armbruster (1997). The points are calorimetric data listed in the reference. **b** The percent difference between the calorimetric heat capacity of spessartine from (**a**) and the lattice heat capacity from vibrational modeling (this work) versus temperature. The variation is less than 1% and is of the same magnitude as seen in other high-temperature calorimetry

a safe estimate for the non-lattice entropy would be about 45 J/mol-K stemming from the expected antiferromagnetic transition. Any further contributions must await experimental confirmation.

Uvarovite: $Ca_3Cr_2Si_3O_{12}$

Of the six endmember silicate garnets, the least is known about the uvarovite component because it is rarely concentrated in garnets above 50%. Recent single-crystal Raman spectroscopy on a synthetic endmember (Chopelas 2005) has allowed a recasting of the thermodynamic model for garnets in order to calculate the lattice contribution to the thermodynamic properties. The calculations for heat capacity and entropy of uvarovite fall between those for almandine and grossular as expected based on the vibrational frequencies found in their respective spectra, particularly the low-energy modes (shown in Fig. 6a, b).

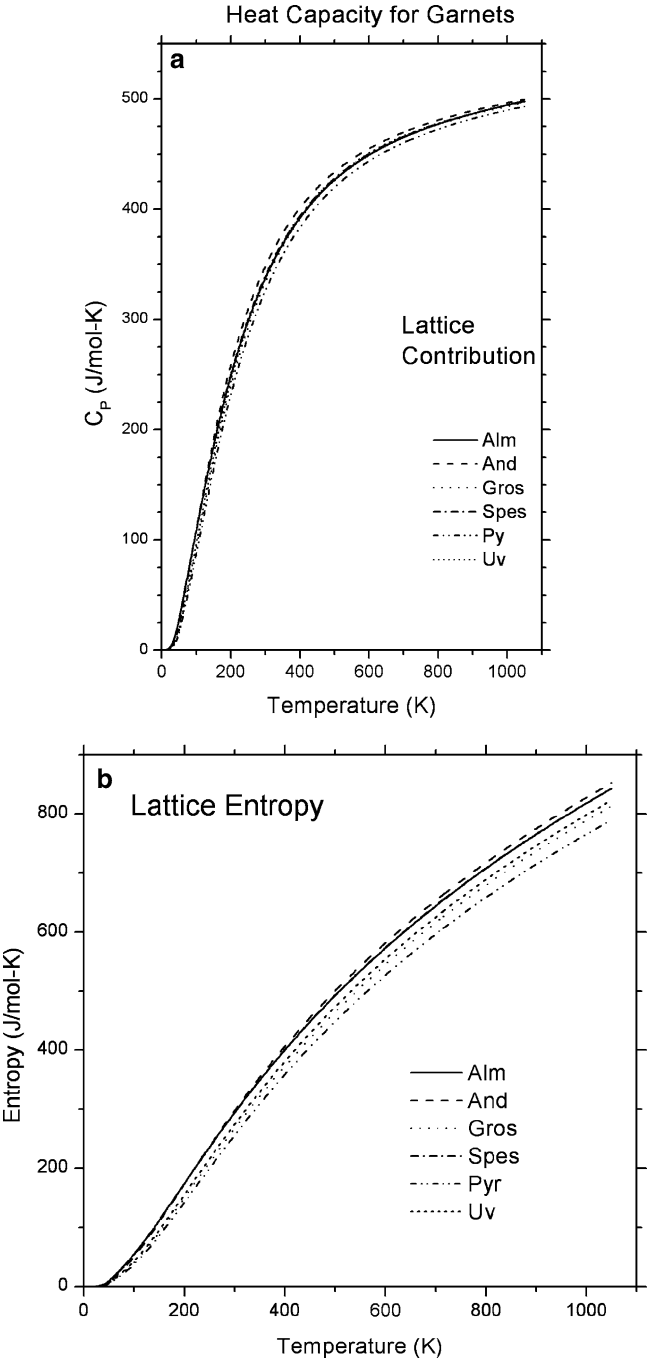

Fig. 6 **a** The lattice heat capacity from vibrational models of all six garnets plotted against temperature. Pyrope is the lowest while andradite is the highest. Uvarovite is between grossular and almandine. **b** The lattice entropies from the vibrational models of all six garnets above room temperature plotted against temperature. Again uvarovite lies between grossular and almandine

Further possible contributions to the thermodynamic properties come from the antiferromagnetic ordering of chromium in the octahedral or Y site. The maximum contribution expected for the entropy is $R \ln(S+1)^2 = 2R \ln 4 = 23.1$ J/mol-K. The Néel temperature should be in the 10–20 K range based on the other garnets.

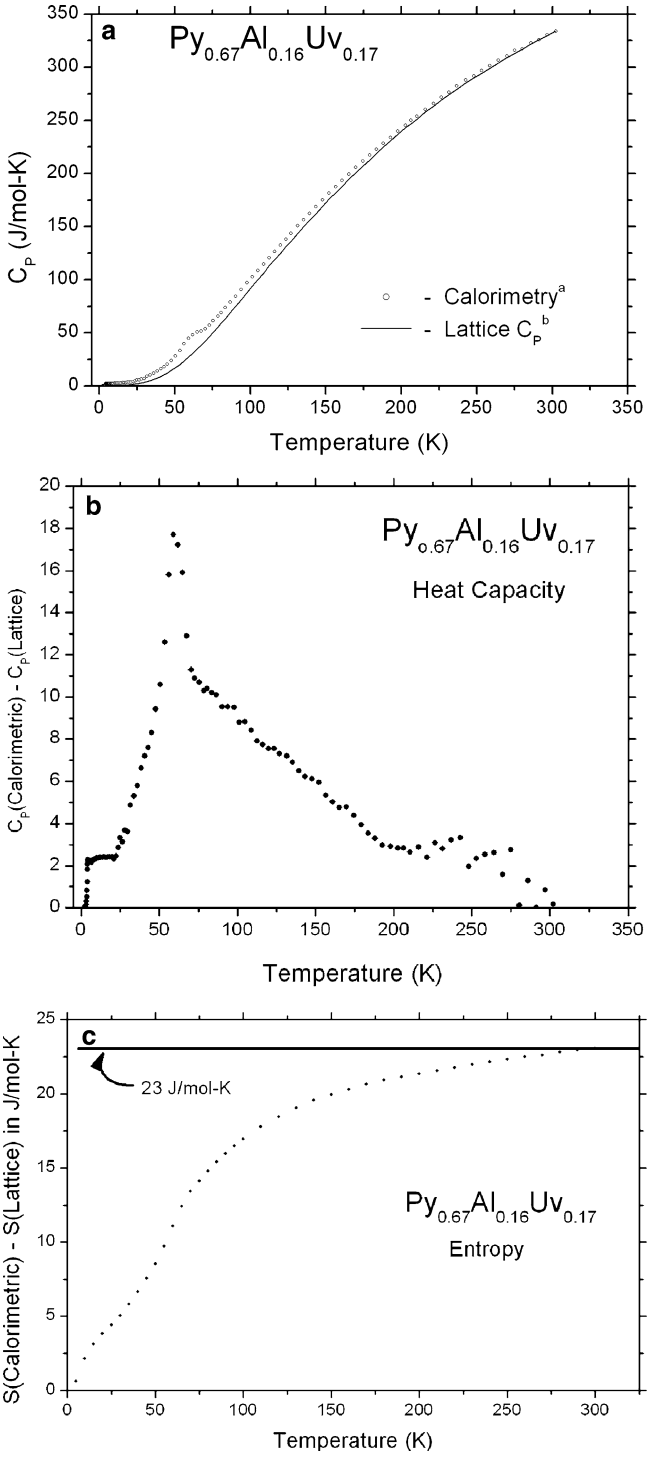

Fig. 7 **a** The calorimetric heat capacity of a ternary garnet ($Py_{0.67}Alm_{0.16}Uv_{0.17}$; Kolesnik et al. 1994) shown as points, plotted with a composite of lattice heat capacities from vibrational modeling against temperature. **b** The difference between the calorimetric heat capacity in (**a**) and the lattice heat capacity of the garnet solid solution ($Py_{0.67}Alm_{0.16}Uv_{0.17}$). The feature at about 8 K is from the antiferromagnetic transition of iron, the broad feature is likely the pyrope non-lattice heat capacity, while the sharp feature at about 60 K most likely represents the antiferromagnetic transition of chromium in uvarovite. Note that the heat capacity difference vanishes at room temperature as it did for andradite and almandine. **c** The difference between the calorimetric entropy and the lattice entropy of the garnet solid solution ($Py_{0.67}Alm_{0.16}Uv_{0.17}$). The non-lattice entropy over the lattice is about 23 J/mol-K by 300 K. Small rises are seen at the antiferromagnetic transition temperatures for iron and chromium, but are not as obvious as those seen in the endmember garnets

However, there is evidence that shows it at approximately 60 K based on low temperature heat capacity measurements of three different garnets with a small uvarovite component (Kolesnik et al. 1994). The garnet with the largest uvarovite component contains 0.17 mol fraction uvarovite, 0.67 pyrope and 0.16 almandine. The large pyrope and almandine contents made it impossible to deduce an unambiguous value for the pure uvarovite magnetic entropy. The lattice contributions from each of the components was multiplied by their mole fraction and summed (0.67 Cp(py) + 0.16 Cp(al) + 0.17 Cp(uv)). Non-ideal effects are not considered here. These results are shown in Fig. 7a with the calorimetric data points (Kolesnik et al. 1994). The difference between the two curves, shown in Fig. 7b, shows a peak at ~60 K. An additional feature ~10 K corresponds to the Néel temperature for almandine, which is ~8 K and a broad feature centered about ~100 K matches that for the non-lattice heat capacity and entropy of pyrope and almandine. The peak at 60 K must be the transition temperature for the trivalent chromium in garnet.

The lattice entropy for this ternary garnet is computed from the heat capacity and compared to the computed entropies from the calorimetric measurements.

When the (vibrational) lattice entropy is subtracted from the (calorimetric) measured entropy, a plateau value of 23 J/mol-K is found for the difference at ~275 K (Fig. 7c). There are several contributions to the difference between the lattice and calorimetric entropies, including entropy of mixing, magnetic entropy of iron and chromium, non-lattice entropy of pyrope (and probably almandine) mentioned earlier, and possible electronic entropy of iron. A simple fractional accounting can be expressed as:

$$\begin{aligned} S(\text{garnet}) - S(\text{lattice}) = {} & S(\text{mixing}) + X_{al}\text{Smag}(Fe^{2+}) \\ & + X_{al}S_{el}(Fe^{2+}) \\ & + X_{uv}\text{Smag}(Cr^{3+}) \\ & + X_{al+py}S(\text{size mismatch}). \end{aligned}$$

Since all these numbers except the magnetic contribution to the entropy by the chromium has been measured (see previous sections), an estimate for the latter should theoretically be possible. However, after adding the known values, with the uncertainties involved in the above estimate, the value for the magnetic contribution to entropy by chromium in uvarovite varies from 0 to 24 J/mol-K. Discovery of the correct contribution will have to await low temperature calorimetry results on end member uvarovite.

Thermodynamic properties at high pressure

One of the strengths of vibrational modeling of thermoelastic properties is the ease at changing the model of a particular mineral at different P,T conditions based on straightforward spectral measurements. There is also clarity as to how the substitution of a cation affects the lattice contribution to heat capacity and entropy. Importantly, it is not expected that changing volume due to changing pressure and/or temperature conditions will greatly affect the magnetic, electronic, or mixing contributions to the thermodynamics of a material. The main changes are expected to be almost solely lattice contributions. Here, the pyralspite garnet minerals may be an exception due to the collapse of the dodecahedral cage at higher pressures. The small change of heat capacity due to this unusual structural feature is unlikely to affect garnet stability at any depth.

High pressure Raman spectra of pyrope, grossular, and andradite (Gillet et al. 1992); A. Chopelas and H.J. Reichmann, unpublished data) and the pressure dependence of acoustic velocities, for example (Chai et al. 1997; Chopelas et al. 1996; Webb 1989) contain enough information to assign pressure shifts to the features in their vibrational models. This shift is expressed as a Grüneisen parameter in Table 1 for the three garnets. If a weighted average of the assigned mode Grüneisen parameters is computed from $\langle \gamma \rangle = \Sigma\ \gamma_i C_i / C_V$, where C_i is the Einstein heat capacity of the ith mode, it yields nearly identical results when the thermal Grüneisen parameter is computed from $\gamma_{th} = \alpha\ K_T V / C_V$ (see Tables 1, 2). It has been noted that in vibrational studies under pressure, the pressure shift of like motions have similar Grüneisen parameters, so groupings of similar molecular motions is a reasonable approximation. When this is applied to the vibrational models (Table 1), the shift in the lattice contributions to the thermodynamic functions is easily obtained. Figure 8a, b shows the heat capacity and entropy results for pyrope to 30 GPa, respectively. As anticipated, at low temperatures, both entropy and heat capacity change little as the volume is collapsed, while the largest changes in these parameters are seen at the highest temperatures.

Once the change in entropy versus pressure is known (Table 3), thermal expansivity can be computed from the Maxwell relation $(\partial S/\partial P)_T = -(\partial V/\partial T)_P$ (Chopelas 1996). For pyrope, grossular, and andradite, this results in 1.6, 1.5, 1.6×10^{-5} K^{-1} at 298 K, respectively, which compares favorably with previous measurements (Isaak et al. 1992; Skinner 1956; Thieblot et al. 1999).

Comparison with petrological databases

Currently, petrological databases, which use the results of calorimetry as well as phase equilibria to make internally consistent datasets, are striving to include pressure effects on the thermodynamic properties. Heat capacity, entropy, and volume are often described as polynomials with respect to temperature. While describing heat capacity as a polynomial is successful for 1 atm work, it is only modestly successful for high-pressure predictions. One such model in wide use is MELTS (Ghiorso and Sack 1995; Ghiorso et al. 2002) which does an excellent job of reproducing the heat capacity of pyrope to the highest temperature of the measurements (Fig. 9). The difficulty in using a polynomial to describe how pressure affects heat capacity and other such properties has been noted often (e.g., Span and Wagner 2003) and is obvious in the figure. Properties may be easily interpolated but not extrapolated. In Fig. 9, at temperatures below 600 K, the

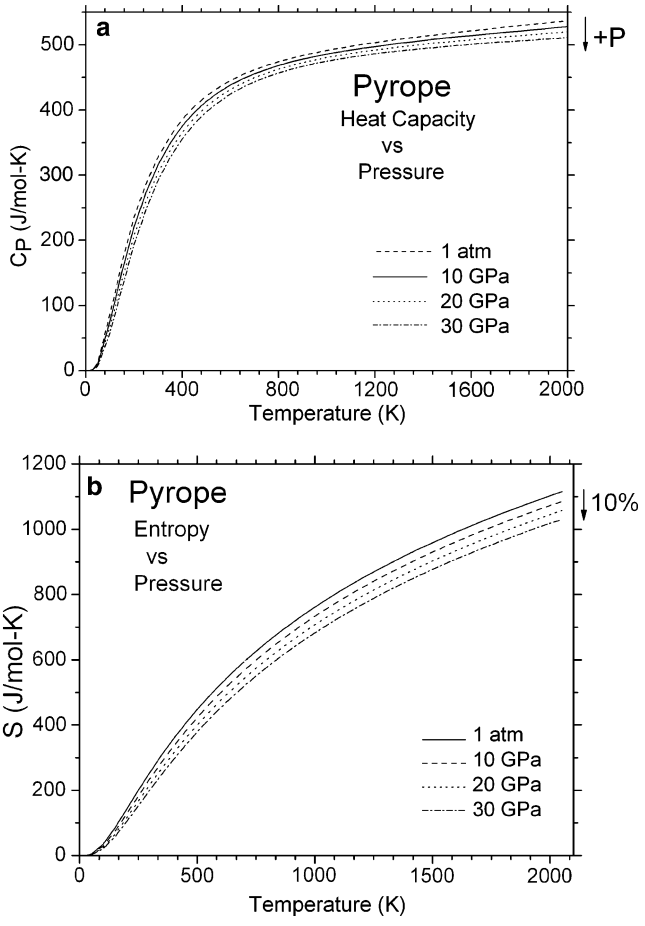

Fig. 8 **a** The lattice heat capacity of pyrope plotted against temperature shown at 1 atm, 10, 20, and 30 GPa. **b** The lattice entropy of pyrope plotted against temperature shown at 1 atm, 10, 20 , and 30 GPa

Table 3 Thermal expansivity at 298 K from vibrational modeling

	dS/dP	$\alpha \times 10^5$ (298 K)	α (lit)
Pyrope	0.182	1.6	1.9
Grossular	0.19	1.5	1.6
Andradite	0.215	1.6	2.0

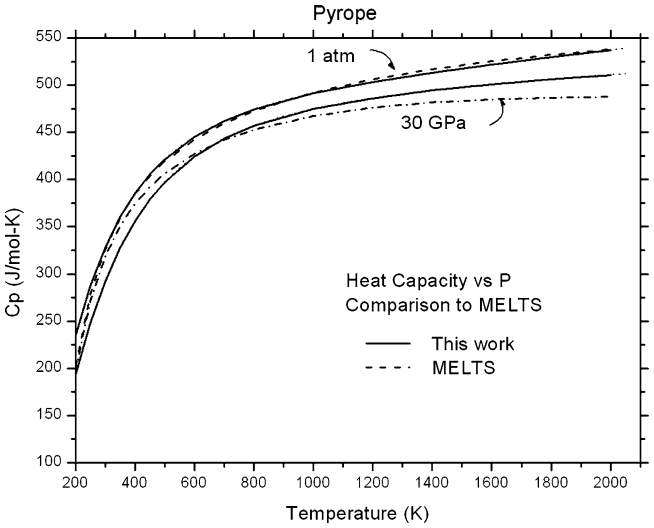

Fig. 9 The heat capacity of pyrope using vibrational modeling (*solid line*) with that calculated using the pMELTS thermodynamic data base (Ghiorso et al. 2002), also known as MELTS (*dashed lines*) plotted versus temperature. At ambient pressures, the heat capacities are very close while at 30 GPa, the pressure dependencies diverge substantially

pressure shift is far too low while at temperatures above 600 K, the pressure shifts are overestimated, by as much as double at mantle relevant temperatures. Clearly, the limits of the model have been exceeded, but this serves to illustrate incorporation of the principles of vibrational modeling into a database for high-pressure estimates would be of great value. Further consistency checks would also be provided by Eqs. 6 and 7.

In summary, vibrational modeling is a powerful method for determining the thermoelastic properties of minerals. Its strength lies in the ability to shift a vibrational model based on simple measurements of spectra at various P–T conditions and compositions. This in turn allows accurate estimates of the lattice contribution to the thermodynamic properties. The pressure dependence of the entropy yields the thermal expansivity, while the pressure derivative of the heat capacity yields the second derivative of the volume with respect to temperature. This allows a further consistency check between the equations of state and the thermodynamic properties.

Acknowledgments I wish to thank C. A. Geiger for sending me his data and fruitful discussions, A. M. Hofmeister for sending me her data prior to publication, J. Ganguly for a thoughtful review, and J. M. Brown for fruitful discussions and critique. This work was supported by NSF grant EAR-0296205.

References

Anderson OL, Isaak DL, Oda H (1991) Thermoelastic parameters for six minerals at high temperature. J Geophys Res 96(B11):18037–18046

Anovitz LM, Essene EJ, Metz GW, Bohlen SR, Westrum EF Jr, Hemingway BS (1993) Heat capacity and phase equilibria of Almandine, $Fe_3Al_2Si_3O_{12}$. Geochim Cosmochim Acta 57:4191–4204

Bass JD (1986) Elasticity of uvarovite and andradite garnets. J Geophys Res 91:7505–7516

Berman RG (1988) Internally-consistent thermodynamic data for minerals in the system Na_2O-K_2O-CaO-MgO-FeO-Fe_2O_3-Al_2O_3-SiO_2- TiO_2-H_2O-CO_2. J Petrol 29:445–522

Berman RG (1990) Mixing properties of Ca-Mg-Fe-Mn garnets. Am Mineral 75:328–344

Boffa Ballaran T, Carpenter MA, Geiger CA, Koziol AM (1999) Local structural heterogeneity in garnet solid solutions. Phys Chem Minerals 26:554–569

Bosenick A, Geiger CA, Cemic L (1996) Heat capacity measurements of synthetic pyrope-grossular garnets between 320 and 1000 K by differential scanning calorimetry. Geochim Cosmochim Acta 60:3215–3227

Chai M, Brown JM, Slutsky LJ (1997) The elastic constants of a pyrope-grossular-almandine garnet to 20 GPa. Geophys Res Lett 24:523–526

Chopelas A (1990b) Thermal expansion, heat capacity, and entropy of MgO at mantle pressures. Phys Chem Minerals 17:142–148

Chopelas A (1990a) Thermal properties of forsterite at mantle pressures derived from vibrational spectroscopy. Phys Chem Minerals 17:149–157

Chopelas A (1991) Thermal properties of β-Mg_2SiO_4 at mantle pressures derived from vibrational spectroscopy: Implications for the mantle at 400 km depth. J Geophys Res B96:11817–11829

Chopelas A (1996) Thermal expansivity of lower mantle phases MgO and $MgSiO_3$ perovskite at high pressure derived from vibrational spectroscopy. Phys Earth Planet Inter 98:3–15

Chopelas A (1999) Estimates of mantle relevant Clapeyron slopes in the $MgSiO_3$ system from high pressure spectroscopic data. Am Mineral 84:233–245

Chopelas A (2000) Thermal expansivity of mantle relevant magnesium silicates from vibrational spectroscopy at high pressures. Am Mineral 85:270–278

Chopelas A (2005) Single-crystal Raman spectroscopy of uvarovite ($Ca_3Cr_2Si_3O_{12}$) garnet. Phys Chem Minerals 32:525–530

Chopelas A, Boehler R, Ko J (1994) Thermodynamics and behavior of γ-Mg_2SiO_4 at high pressure: Implications for Mg_2SiO_4 phase equilibrium. Phys Chem Minerals 21:351–359

Chopelas A, Reichmann HJ, Zhang L (1996) Sound velocities of five minerals to mantle pressures determined by the sideband fluorescence method. In: Dyar MD, McCammon C, Schaeffer MW (eds) Mineral spectroscopy: a tribute to Roger G Burns, vol. The Geochemical Society, Houston, pp 229–242

Drulis M, Iwasieczko W, Wolcyrz M, Drulis H (2002) Low-temperature specific heat of non-stoichiometric β-ytterbium deuteride. J Alloys Comp 337:64–68

Fabrichnaya OB (1995) Thermodynamic data for phases in the FeO-MgO-SiO_2 system and phase relations in the mantle transition zone. Phys Chem Minerals 22:323–332

Fei Y, Saxena SK, Navrotsky A (1990) Internally consistent thermodynamic data and equilibrium phase relations for compounds in the system MgO-SiO_2 at high pressure and high temperature. J Geophys Res B95:6915–6928

Ganguly J, Saxena SK (1987) Mixtures and mineral reactions, vol 19. Springer, Berlin, Heidelberg New York

Ganguly J, Cheng W, Tirone M (1996) Thermodynamics of aluminosilicate garnet solid solution; new experimental data, an optimized model, and thermometry applications. Contrib Mineral Petrol 126(1–2):137–151

Geiger CA (1998) AA powder infrared spectroscopic investigation of garnet binaries in the system $Mg_3Al_2Si_3O_{12}$–$Fe_3Al_2Si_3O_{12}$–$Mn_3Al_2Si_3O_{12}$–$Ca_3Al_2Si_3O_{12}$. Eur J Mineral 10(3):407–422

Geiger CA, Armbruster T (1997) $Mn_3Al_2Si_3O_{12}$ spessartine and $Ca_3Al_2Si_3O_{12}$ grossular garnet; structural dynamic and thermodynamic properties. Am Mineral 82(7–8):740–747

Ghiorso MS, Sack RO (1995) Chemical mass transfer in magmatic processes IV: a revised and internally consistent thermodynamic model for the interpolation and extrapolation of liquid–solid

equilibria in magmatic systems at elevated temperatures and pressures. Contrib Mineral Petrol 119:197–212
Ghiorso MS, Hirshmann MM, Reiners PW, Kress VC (2002) The pMELTS: the revision of MELTS for improved calculation of phase boundaries and major element partitioning related to partial melting of the mantle to 3 GPa. Geoch Geophys Geosyst 3(5):1030
Gillet P, Richet P, Guyot F, Fiquet G (1991) High-temperature thermodynamic properties of forsterite. J Geophys Res B 96:11805–11816
Gillet P, Fiquet G, Malezieux JM, Geiger CA (1992) High-pressure and high-temperature Raman spectroscopy of end-member garnets; pyrope, grossular and andradite. Eur J Mineral 4(4):651–664
Grevel KD, Navrotsky A, Kaul WA, Faßhauer DW, Majzlan J (2001) Thermodynamic data of the high-pressure phase $Mg_5Al_5Si_6O_{21}(OH)_7$ (Mg-surasaaite). Phys Chem Minerals 28:475–487
Haselton HT Jr, Westrum EF Jr (1980) Low temperature heat capacities of synthetic pyrope, grossular, and $pyrope_{60}grossular_{40}$. Geochim Cosmochim Acta 44:701–709
Hofmeister AM (1987) Single-crystal absorption and reflection infrared spectroscopy of forsterite and fayalite. Phys Chem Minerals 14:499–513
Hofmeister AM (1996) Thermodynamic properties of stishovite at mantle conditions determined from pressure variations of vibrational modes. In: Dyar MD, McCammon C, Schaefer MW (eds) Mineral spectroscopy: a tribute to Roger G Burns. The Geochemical Society, Houston, pp 215–227
Hofmeister AM, Chopelas A (1991a) Thermodynamic properties of pyrope and grossular from vibrational spectroscopy. Am Mineral 76:880–891
Hofmeister AM, Chopelas A (1991b) Vibrational spectroscopy of end-member silicate garnets. Phys Chem Minerals 17:503–526
Hofmeister AM, Fagan TJ, Campbell KM, Schaal RB (1996) Single-crystal IR spectroscopy of pyrope-almandine garnets with minor amounts of Mn and Ca. Am Mineral 81:418–428
Holland TJB, Powell R (1998) An internally-consistent thermodynamic dataset for phases of petrological interest. J Met Petrol 16:309–343
Isaak DG, Anderson OL, Oda H (1992) High-temperature thermal expansion and elasticity of calcium-rich garnets. Phys Chem Minerals 19:106–120
Kolesnik YN, Yachmenev VY, Vilkovskiy VA, Vishnevskiy AA (1994) Heat capacity of 2–300 K temperature range and entropy of chromium-bearing garnets. Geokhimiya 1994(1):89–100
Kolesov BA, Geiger CA (1998) Raman spectra of silicate garnets. Phys Chem Minerals 25:142–151
Kolesov BA, Geiger CA (2000) Low-temperature single-crystal Raman spectrum of pyrope. Phys Chem Minerals 27:645–649
Krupka KM, Robie RA, Hemingway BS (1979) High temperature heat capacities of corundum, periclase, anorthite, $CaAl_2Si_2O_8$ glass, muscovite, pyrophyllite, $KalSi_2O_8$ glass, grossular and $NaAlSi_3O_8$ glass. Am Mineral 64:86–101
Kuskov OL, Galimzyanov RF, Khitarov NI, Urusov VS (1983) Phase relationships in the MgO–SiO_2 system at the P–T conditions of the mantle transition zone (Translated). Geokhimiya 8:1075–1091
McAloon BP, Hofmeister AM (1995) Single-crystal IR spectroscopy of grossular-andradite garnets. Am Mineral 80:1145–1156
Moore RK, White WB (1971) Vibrational spectra of the common silicates: I. The garnets. Am Mineral 56:54–71
Robie RA, Hemingway BS, Takei H (1982) Heat capacities and entropies of Mg_2SiO_4, Mn_2SiO_4, and Co_2SiO_4 between 5 and 380 K. Am Mineral 67(5–6):470–482
Robie RA, Haselton HT, Hemingway BS (1984) Heat capacities and entropies of rhodochrosite ($MnCO_3$) and siderite ($FeCO_3$) between 5 and 600 K. Am Mineral 69(3–4):349–357
Robie RA, Bin Z, Hemingway BS, Barton MD (1987) Heat capacity and thermodynamic properties of andradite garnet, $Ca_3Fe_2Si_3O_{12}$, between 10 and 1000 K and revised values for $\Delta_f G^0_m$ (298.15 K) of hedenbergite and wollastonite. Geochim Cosmochim Acta 51:2219–2224
Robie RA, Huebner JS, Hemingway BS (1995) Heat capacities and thermodynamic properties of braunite (Mn_7SiO_{12}) and rhodonite ($MnSiO_3$). Am Mineral 80(5–6):560–575
Rodehorst U, Carpenter MA, Boffa Ballaran T, Geiger CA (2004) Local structural heterogeneity, mixing behaviour and saturation effects in the grossular–spessartine solid solution. Phys Chem Minerals 31(7):387–404
Savage FS, Chopelas A (2002) Single crystal Raman spectroscopy and thermodynamics of garnet solid solutions I: Grossular–Andradite. EOS Trans Am Geophys U (abstract)
Savage FS, Chopelas A (2003) Single crystal Raman spectroscopy and thermodynamics of garnet solid solutions II: Pyrope–Almandine binary. EOS Trans Am Geophys U (abstract, Fall 2003)
Saxena SK, Chatterjee N, Fei Y, Shen G (1993) Thermodynamic data on oxides and silicates, vol. Springer, Berlin, Heidelberg New York p 428
Skinner BJ (1956) Physical properties of end-members of the garnet group. Am Mineral 41:428–436
Span R, Wagner W (2003) Equations of state for technical applications. I. Simultaneously optimized functional forms for polar and non polar fluids. Int J Thermophys 24(1):1–36
Tequi C, Robie RA, Hemingway BS, Neuville DR, Richet P (1991) Melting and thermodynamic properties of pyrope ($Mg_3Al_2Si_3O_{12}$). Geochim Cosmochim Acta 55(4):1005–1010
Thieblot L, Tequi C, Richet P (1999) High-temperature heat capacity of grossular ($Ca_3Al_2Si_3O_{12}$), enstatite ($MgSiO_3$), and titanite ($CaTiSiO_5$). Am Mineral 84(5):848–855
Ulbricht HH, Waldbaum DR (1976) Structural and other contributions to third law entropies of silicates. Geochim Cosmochim Acta 40(1):1–24
Webb SL (1989) The elasticity of the upper mantle orthosilicates olivine and garnet to 3 GPa. Phys Chem Minerals 89(7):684–692
Wood BJ (1981) Crystal field electronic effects on the thermodynamic properties of Fe^{2+} minerals. In: Newton RCN, A, Wood, BJ (eds) Thermodynamics of minerals and melts, vol 1. Springer, Berlin Heidelberg New York, pp 63–84
Zhang L, Ahsbahs H, Kutoglu A (1998) Hydrostatic compression and crystal structure of pyrope to 33 GPa. Phys Chem Minerals 25(4):301
Zhang L, Ahsbahs H, Kutoglu A, Geiger CA (1999) Single-crystal hydrostatic compression of synthetic pyrope, almandine, spessartine, grossular, and andradite garnets at high pressure. Phys Chem Minerals 27:52–58